Chirally motivated in-medium $\bar{K}$N amplitudes

Aleš Cieplý

Nuclear Physics Institute, Řež/Prague, Czechia

model formulated with J. Smejkal

acknowledged collaboration with E. Friedman, A. Gal, D. Gazda, J. Mareš

Future Prospects of Hadron Physics, J-PARC, Feb 9, 2012

Outline

A.C., J. Smejkal - Nucl. Phys. A (2012), arXiv:1112.0917

A.C., E. Friedman, A. Gal, D. Gazda, J. Mareš - Phys. Lett. B 702 (2011) 402, Phys. Rev. C 84 (2011) 045206

Introduction

$\bar{K}N$ interaction

strongly interacting multichannel system with an s-wave resonance, the $\Lambda(1405)$, just below the K^-p threshold

$\downarrow\downarrow\downarrow$

$\bar{K}$-nucleus interaction

strongly attractive and absorptive, $V_{\rm opt}(\rho) \sim t_{\bar{K}N}(\rho)\,\rho$

? optical potential depth: phenomenology $V_{\rm opt}$=**(150-200)** MeV
chiral models $V_{\rm opt}$=**(50-60)** MeV

? existence of sufficiently narrow K^-–nuclear bound states

$\downarrow\downarrow\downarrow$

kaon propagation in nuclear matter

heavy ion collisions

? kaon condensation, neutron star structure

Introduction

A modern theoretical treatment of $\bar{K}N$ interaction is based on an effective chiral Lagrangian (a concept introduced by Weinberg for the πN interaction)

- CHPT implements the QCD symmetries in it's nonperturbative regime
- coupled channels techniques are used to deal with divergencies due to resonances in the strangeness $S = -1$ sector
- $\Lambda(1405)$ resonance generated dynamically; two $I = 0$ poles
- the leading order Tomozawa-Weinberg interaction does surprisingly well but NLO terms are necessary to achieve a good qualitative reproduction of the low energy K^-p data
- new precise data on the 1s energy level characteristics in the kaonic hydrogen atom from SIDDHARTA experiment (plus the kaonic deuterium should follow soon)

OUR WORK: simultaneous description of the K-atomic and low energy K^-p data to fix model parameters, then the model is used to study meson-baryon resonances and in-medium properties of the $\bar{K}N$ system

Separable meson-baryon potentials

the model describes interactions of the lightest meson and baryon octets:

$$\phi = \begin{pmatrix} \pi^0 + \frac{1}{\sqrt{3}}\eta & \sqrt{2}\pi^+ & \sqrt{2}K^+ \\ \sqrt{2}\pi^- & -\pi^0 + \frac{1}{\sqrt{3}}\eta & \sqrt{2}K^0 \\ \sqrt{2}K^- & \sqrt{2}\bar{K}^0 & -\frac{2}{\sqrt{3}}\eta \end{pmatrix} \qquad B = \begin{pmatrix} \frac{1}{\sqrt{2}}\Sigma^0 + \frac{1}{\sqrt{6}}\Lambda & \Sigma^+ & p \\ \Sigma^- & -\frac{1}{\sqrt{2}}\Sigma^0 + \frac{1}{\sqrt{6}}\Lambda & n \\ \Xi^- & \Xi^0 & -\frac{2}{\sqrt{6}}\Lambda \end{pmatrix}$$

10 coupled $Q = 0$ channels:	$\pi^0\Lambda$	$\sim$ 1250 MeV
	$\pi^0\Sigma^0$, $\pi^-\Sigma^+$, $\pi^+\Sigma^-$	$\sim$ 1330 MeV
	K^-p, $\bar{K}^0n$	$\sim$ 1430 MeV
	$\eta\Lambda$, $\eta\Sigma^0$	$\sim$ 1700 MeV
	$K^0\Xi^0$, $K^+\Xi^-$	$\sim$ 1800 MeV
6 coupled $Q = -1$ channels:	$\pi^-\Lambda$	$\sim$ 1250 MeV
	$\pi^-\Sigma^0$, $\pi^0\Sigma^-$	$\sim$ 1330 MeV
	K^-n	$\sim$ 1430 MeV
	$\eta\Sigma^-$	$\sim$ 1700 MeV
	$K^0\Xi^-$	$\sim$ 1800 MeV

Separable meson-baryon potentials

We employ the effective chiral model of Kaiser, Siegel and Weise (1995) with the s-wave meson-baryon Lagrangian up to the second order, the heavy baryon formulation

Parameters: f_π, f_K, f_η - meson decay constants

M_0 - baryon octet mass

$D \simeq 3/4$, $F \simeq 1/2$ - axial vector couplings, $g_A = F + D$

b_0, b_D, b_F, four d's - second order couplings

Schematic picture (taken from Borasoy, Nissler, Weise - 2005):

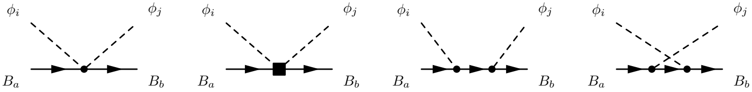

$\mathcal{O}(q^1)$ contact $\mathcal{O}(q^2)$ contact direct s-term crossed u-term

Separable meson-baryon potentials

Problem: χPT is not applicable in the resonance region!
Solution: effective separable potentials constructed to match the chiral amplitudes up to $\mathcal{O}(q^2)$

$$V_{ij}(k,k';\sqrt{s}) = \sqrt{\frac{1}{2\omega_i}\frac{M_i}{E_i}}\, g_i(k^2)\, \frac{C_{ij}(\sqrt{s})}{f_i\, f_j}\, g_j(k'^2) \sqrt{\frac{1}{2\omega_j}\frac{M_j}{E_j}}$$

Lippmann-Schwinger equation used to solve exactly the loop series

- kinematical factors guarantie a proper relativistic flux normalization with ω_i, M_i and E_i denoting the meson energy, the baryon mass and energy in the meson-baryon CMS
- coupling matrix C_{ij} determined by the chiral SU(3) symmetry, includes terms up to second order in the meson c.m. kinetic energies
- the formfactors $g_j(k) = 1/[1 + (k/\alpha_j)^2]$ account naturally for the off-shell effects with the inverse ranges α_j fitted to the low energy $\bar{K}N$ data
- our approach differs from the more popular on-shell scheme based on the Bethe-Salpeter equation and the unitarity relation for the inverse of the T-matrix

Separable meson-baryon potentials

The resulting meson-baryon amplitudes are of the separable form:

$$F_{ij}(p,p';\sqrt{s}) = -\frac{g_i(p)g_j(p')}{4\pi\, f_i\, f_j}\sqrt{\frac{M_i M_j}{s}}\left[(1 - C(\sqrt{s})\cdot G(\sqrt{s}))^{-1}\cdot C(\sqrt{s})\right]_{ij}$$

where the meson-baryon propagator $G(\sqrt{s})$ is diagonal in the channel indices i and j,

$$G_i(\sqrt{s};\rho) = \frac{1}{f_i^2}\frac{M_i}{\sqrt{s}}\int_{\Omega_i(\rho)}\frac{d^3\vec{p}}{(2\pi)^3}\frac{g_i^2(p)}{p_i^2 - p^2 - \Pi_i(\omega_i, E_i, \vec{p};\rho) + \mathrm{i}0}$$

- integration domain $\Omega_i(\rho)$ is limited by the Pauli principle in the $\bar{K}N$ channels
- Π_i represents a sum of meson and baryon self-energies in channel i
- $\Pi_{\bar{K}} \sim F_{\bar{K}N}\,\rho \;\Rightarrow\;$ selfconsistent treatment required

Data reproduction

Threshold branching ratios:

$$\gamma = \frac{\sigma(K^-p \to \pi^+\Sigma^-)}{\sigma(K^-p \to \pi^-\Sigma^+)} = 2.36 \pm 0.04 \ ,$$

$$R_c = \frac{\sigma(K^-p \to \text{charged particles})}{\sigma(K^-p \to \text{all})} = 0.664 \pm 0.011 \ ,$$

$$R_n = \frac{\sigma(K^-p \to \pi^0\Lambda)}{\sigma(K^-p \to \text{all neutral states})} = 0.189 \pm 0.015.$$

K^-p cross sections to six different meson-baryon final states:

at the $p_{LAB} = 110$ MeV for the K^-p, $\bar{K}^0 n$, $\pi^+\Sigma^-$, $\pi^-\Sigma^+$
at the $p_{LAB} = 200$ MeV for the above channels plus $\pi^0\Lambda$, $\pi^0\Sigma^0$

Data reproduction

Kaonic hydrogen characteristics:

strong interaction energy shift	$\Delta E_N(1s)$
the decay width	$\Gamma(1s)$

two recent measurements at at DAΦNE in Frascati:

DEAR (2005)	$\Delta E_N(1s) = 193 \pm 37(stat.) \pm 6(syst.)$ eV $\Gamma(1s) = 249 \pm 111(stat.) \pm 39(syst.)$ eV
SIDDHARTA (2011)	$\Delta E_N(1s) = 283 \pm 36(stat.) \pm 6(syst.)$ eV $\Gamma(1s) = 541 \pm 89(stat.) \pm 22(syst.)$ eV

our approach - direct numerical solution of the $K^- p$ bound state problem, no Deser-like relation to the $K^- p$ scattering length

Data reproduction

Fit to 15 experimental data:
3 branching ratios, 2 kaonic hydrogen characteristics, 10 cross sections

- **TW1** only the leading order (LO) Tomozawa-Weinberg interaction,
  two parameters: $\alpha_i = \alpha_{TW} = 701$ MeV, $f_i = f_{TW} = 113$ MeV
- **NLO30** LO+NLO interactions, couplings f_i fixed at physical values
  $f_\pi = 92.4$ MeV, $f_K = 110.0$ MeV and $f_\eta = 118.8$ MeV,
  inverse ranges of channels closed at the $\bar{K}N$ threshold set to
  $\alpha_{\eta\Lambda} = \alpha_{\eta\Sigma^0} = \alpha_{K\Xi} = 700$ MeV;
  fitted 3 inverse ranges and 4 NLO d–couplings
- **CS30** LO+NLO model taken from our previous work, included DEAR data instead of SIDDHARTA

inverse ranges (in MeV) and d–couplings (in GeV^{-1}):

model	$\alpha_{\pi\Lambda}$	$\alpha_{\pi\Sigma}$	$\alpha_{\bar{K}N}$	d_0	d_D	d_F	d_1
CS30	291	601	639	−0.450	0.026	−0.601	0.235
NLO30	297	491	700	−0.812	0.288	−0.737	−0.016

Data reproduction

$K^- p$ threshold data calculated in several LO and LO+NLO coupled-channel chiral models.

model	ΔE_{1s}	Γ_{1s}	γ	R_c	R_n	z_1(I=0)	z_2(I=0)
TW1	323	659	2.36	0.636	0.183	(1371, −54)	(1433, −25)
JOR	275*	586*	2.30	0.618	0.257	(1389, −64)	(1427, −17)
IHW	373*	495*	2.36	0.66	0.20	(1384, −90)	(1422, −16)
NLO30	310	607	2.37	0.660	0.191	(1355, −86)	(1418, −44)
CS30	260	692	2.37	0.655	0.188	(1398, −51)	(1441, −76)
BNW	236*	580*	2.35	0.653	0.194	(1408, −37)	(1449, −106)
IHW	306*	591*	2.37	0.66	0.19	(1381, −81)	(1424, −26)
exp.	283	541	2.36	0.664	0.189	–	–
error (±)	42	111	0.04	0.011	0.015	–	–

Data reproduction

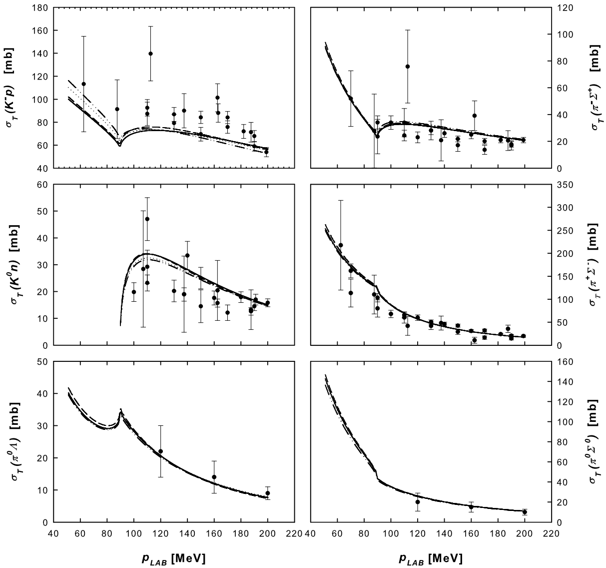

Data reproduction

$\pi\Sigma$ mass distribution: comparison with results taken from three "compatible" experiments:

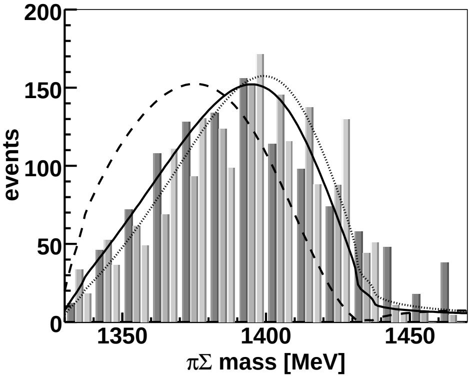

$$dN_{\pi\Sigma}/dM \sim \left| T_{\pi\Sigma,\pi\Sigma}(I=0) + r_{KN/\pi\Sigma}\; T_{\pi\Sigma,\bar{K}N}(I=0) \right|^2 p_{\pi\Sigma}$$

Free space and in-medium $\bar{K}N$ amplitudes

Energy dependence of the real (left panel) and imaginary (right panel) parts of the elastic $K^- p$ amplitude in the free space. Dashed curves: TW1 model, dot-dashed: CS30 model, solid curves: NLO30 model.

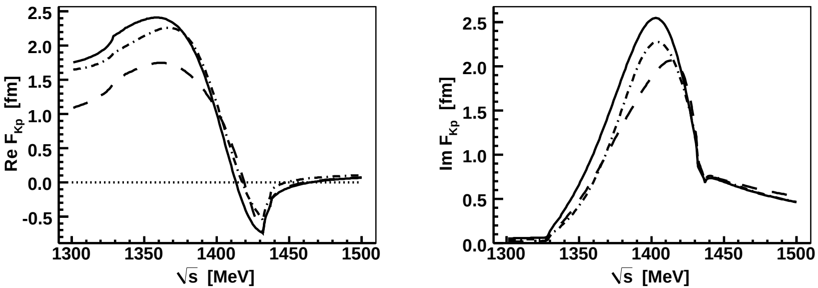

Free space and in-medium $\bar{K}N$ amplitudes

Energy dependence of the real (left panel) and imaginary (right panel) parts of the elastic $K^- p$ amplitude in nuclear medium at the nuclear density $\rho = \rho_0$. Dashed curves: TW1 model, dot-dashed: CS30 model, solid curves: NLO30 model.

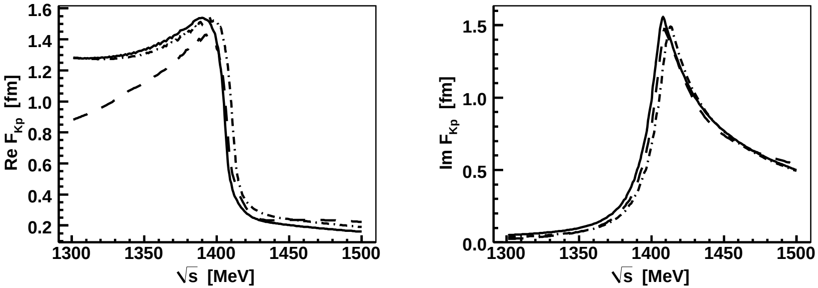

Free space and in-medium $\bar{K}N$ amplitudes

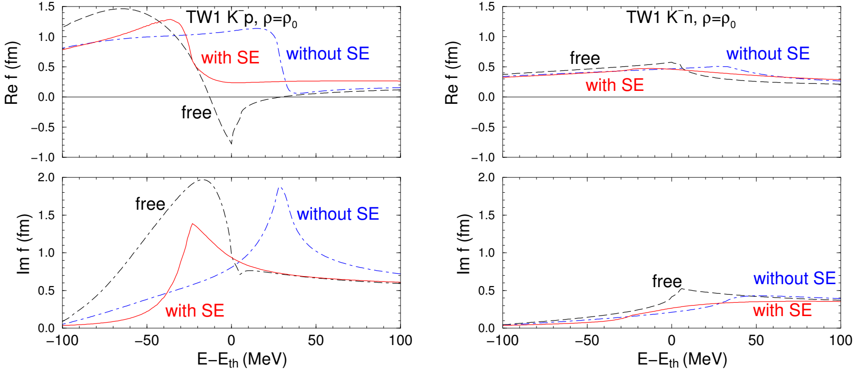

Energy dependence of the c.m. reduced amplitudes f_{K^-p} (left panels) and f_{K^-n} (right panels) in our TW1 model. The upper and lower panels refer to the real and imaginary parts of the $\bar{K}N$ amplitudes, respectively. Dashed curves: free space, dot-dashed: Pauli blocked amplitude (without SE) at $\rho = \rho_0$, solid curves: including meson and baryon self energies (with SE) at $\rho = \rho_0$.

In-medium pole movements

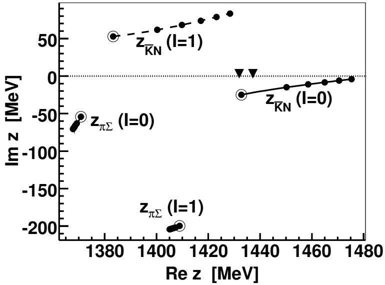

upper half (above real axis):
$[+,-]$ Riemann sheet (the third RS), no quasibound interpretation of the poles

lower half (below real axis):
$[-,+]$ Riemann sheet (the second RS) accessible from the physical region by crossing the real energy axis in between the $\pi\Sigma$ and $\bar{K}N$ thresholds

Pole movements on the complex energy manifold due to the increased effect of Pauli blocking. There are two I=0 poles and two I=1 poles. The pole trajectories were calculated from the free-space pole positions (encircled dots) up to the pole positions at full nuclear density ρ_0. The solid triangles denote the $K^- p$ and $\overline{K^0} n$ thresholds. The movement of the $z_{\bar{K}N}$(I=0) pole demonstrates how the properties of in-medium $\bar{K}N$ interaction are related to the dynamics of the $\Lambda(1405)$ resonance in the nuclear medium.

$\bar{K}$-nuclear optical potential

single nucleon approximation, a coherent sum of $\bar{K}N$ interactions:

$$V_{K^-} = -\frac{2\pi}{\omega_K}\,(1+\frac{\omega_K}{m_N})\,F_{K^-N}(\vec{p},\sqrt{s};\rho)\,\rho$$

The kaons interacting with nuclei probe the subthreshold energy region!
two-body c.m. system: $\vec{p}_K + \vec{p}_N = \vec{0}$
K^-–nucleus c.m. system: $\vec{p}_K + \vec{p}_N \neq \vec{0}$

bound hadrons, averaging over angles, local density approximation, Fermi gas model:

$$\sqrt{s} \approx E_{\rm th} - B_N - \frac{m_N}{m_N+m_K}\,B_K - 15.1\,(\rho/\rho_0)^{2/3} + \frac{m_K}{m_N+m_K}\,{\rm Re}\,\mathcal{V}_{K^-}(\rho)\ \ \text{(in MeV)}$$

in nuclear medium, one has to use realistic momenta in the form factors $g_i(p)$

$$p^2 \approx \frac{m_K m_N}{(m_N+m_K)^2}[2m_K T_N(\rho/\rho_0)^{2/3} - 2m_N(B_K + {\rm Re}\,\mathcal{V}_{K^-}(\rho))],$$

A.C., E. Friedman, A. Gal, D. Gazda, J. Mareš - PRC84 (2011) 045206

$\bar{K}$-nuclear optical potential

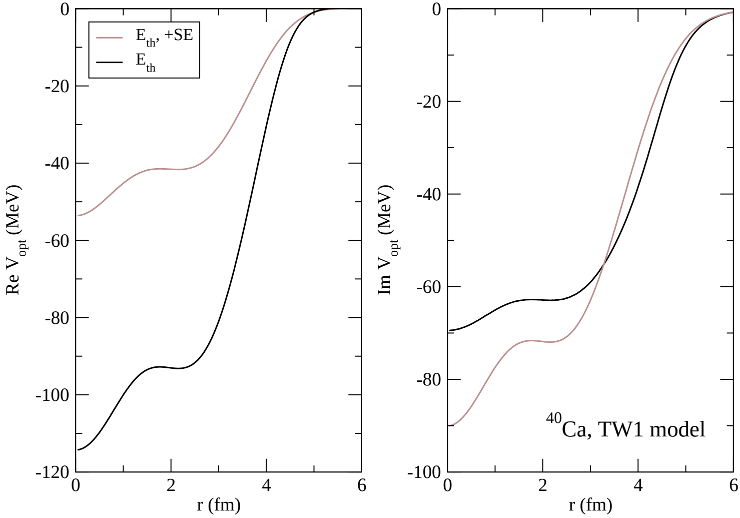

$\bar{K}$-nuclear optical potential

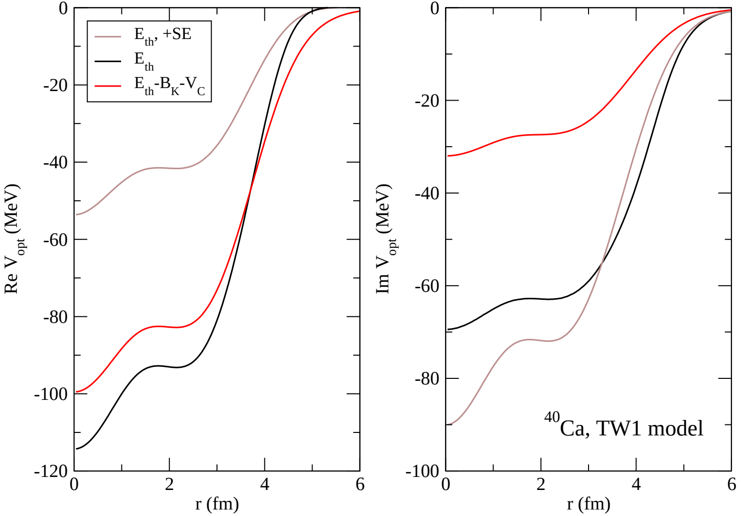

$\bar{K}$-nuclear optical potential

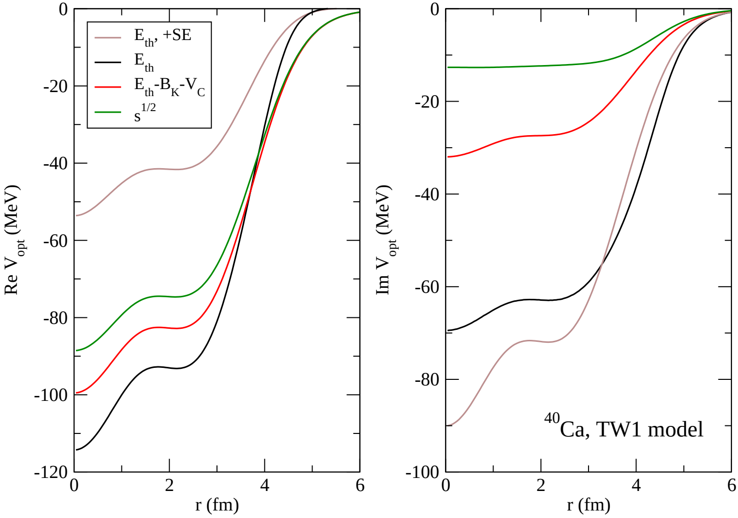

$\bar{K}$-nuclear optical potential

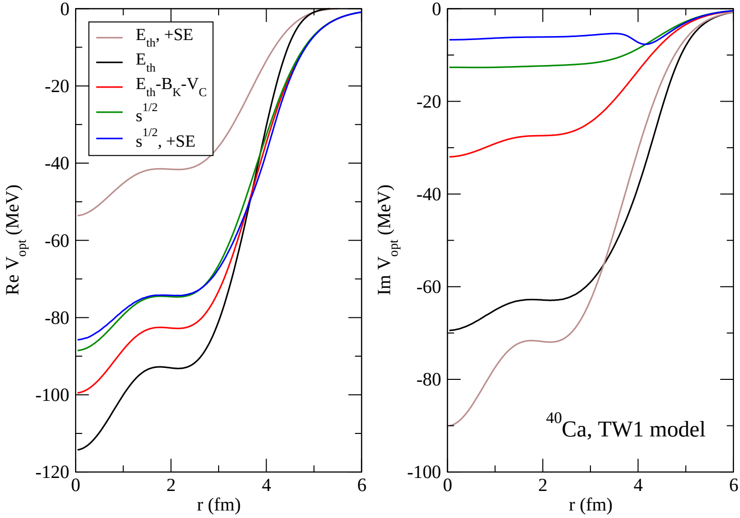

calculations by D. Gazda, J. Mareš, to appear in Nucl. Phys. A (2012)

$\bar{K}$-nuclear optical potential

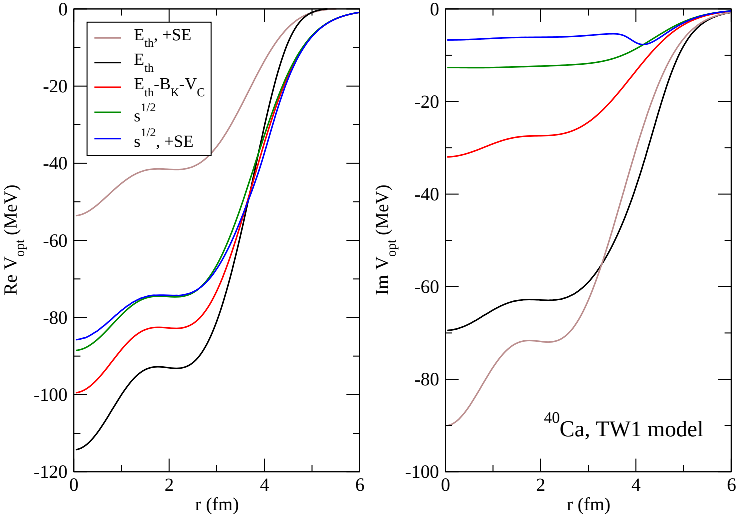

calculations by D. Gazda, J. Mareš, to appear in Nucl. Phys. A (2012)

Summary

- The in-medium dynamics of the $\Lambda(1405)$ resonance is responsible for the rapid increase of the real part of our $K^- p$ amplitude at energies about 30 MeV below the $\bar{K}N$ threshold.
- The Pauli blocking pushes the resonance structure above the threshold and the kaon self-energy is responsible for moving it back to energies where it is located in the free space.
- The observed sharp increase of $K^- p$ in-medium attraction below the $\bar{K}N$ threshold is a robust feature common to all considered models.
- The construction of the optical potential from subthreshold $\bar{K}N$ energies allows to link the shallow $\bar{K}$-nuclear potentials based on the chiral $\bar{K}N$ amplitude evaluated at threshold and the deep phenomenological optical potentials obtained in fits to kaonic atoms.
- New measurements of $K^- p \longrightarrow \pi^0 \Lambda$ and $K^- p \longrightarrow \pi^0 \Sigma^0$ reactions at low kaon energies would be highly appreciated.